

# Statistical methods for assessing the dimensions of synaptic vesicles in nerve terminals

A. Feuerverger<sup>a</sup>, M. Menzinger<sup>b</sup>, H.L. Atwood<sup>c</sup>, R.L. Cooper<sup>d,\*</sup>

<sup>a</sup> Department of Statistics, University of Toronto, Toronto, Ont., Canada, 5MS 3G3

<sup>b</sup> Department of Physical Chemistry, University of Toronto, Toronto, Ont., Canada, M5S 3H6

<sup>c</sup> Department of Physiology, University of Toronto, Toronto, Ont., Canada, 5MS 1A8

<sup>d</sup> 101 Morgan Building, T.H. Morgan School of Biological Sciences, University of Kentucky, Lexington, KY 40506-0225, USA

Received 24 February 2000; received in revised form 14 August 2000; accepted 15 August 2000

## Abstract

Chemical transmission between neurons occurs by the release of neurotransmitter packaged within vesicles of the presynaptic neuron onto a postsynaptic target. The amount of transmitter contained within a vesicle is in part regulated by the size of the vesicle. Thus, it is of general interest to quantify the dimension of vesicles in understanding the basic principles of chemical synaptic transmission. These vesicles can only be measured by electron microscopic techniques. Obtaining the true dimensions of synaptic structures is therefore complicated by stereological considerations. In this study, we suggest improved methods for determining the distributions (and mean sizes) for populations of vesicle diameters by mathematical processes involving (1) an implicit inversion of the empirical data distribution, (2) an explicit inversion approach, and (3) an approach based on substituting the empirical distribution into the inversion formula and then isotonzing using an iterated convex minorant algorithm. These procedures provide distributions that better represent the true population distributions (and means) for comparisons with other data sets of vesicle diameter measures. © 2000 Elsevier Science B.V. All rights reserved.

**Keywords:** Nerve; Vesicles; Sterology; Synapse; Morphology

## 1. Introduction

Characterizing structural entities of synapses, which mediate communication between nerve cells and their targets is important for defining the limits of cellular interactions. Synaptic vesicles within nerve terminals package and store neurotransmitter substances and when released during exocytosis, cause a reaction in the receiving (postsynaptic) cells. Synaptic vesicles are concentrated within the presynaptic nerve terminal and release their contents when there is an intracellular rise of calcium ions ( $\text{Ca}^{2+}$ ) in the nerve terminal due to electrical depolarization. The amount of neurotransmitter stored and released by a vesicle is one of the factors that influences the size of the postsynaptic response

(Zhang et al., 1998). Thus, changes in the size of synaptic vesicles through genetic or physiological alterations have important implications for neuronal signaling. For example, stimulation in the hippocampus of rats to induce long-term potentiation induced depletion of transmitter and a reduction in the observable vesicle diameters within the presynaptic terminals. The reduction in vesicle size was reversible when physiological recovery resumed (Petukhov and Popov, 1986). Also, in *Drosophila*, recent studies of mutants have shown that quantal size is related to vesicle size. Examples include the *shibire* mutation, in which the vesicles become increased in size (van de Goor et al., 1995; Zhang et al., 1998). Increasingly, genetic mutations which effect synaptic function are being studied in *Drosophila*, and the relationship between synaptic structure and function requires precise assessment of synaptic structures and matching dimensions of synaptic vesicles (Atwood and Cooper, 1995; Cooper et al., 1995a,b, 1996; Propst and Ko, 1987; Wong et al., 1999).

\* Corresponding author. Tel.: +1-859-2575050; fax: +1-859-2571717.

E-mail address: RLCOOP1@pop.uky.edu (R.L. Cooper).

In order to assess such structure–function relationships, careful measure of synaptic vesicles and the limitations of this measurement need to be addressed. However, measurement of vesicular dimensions is particularly problematic because of their small size; they can only be visualized for measurement in micrographs obtained by electron microscopy. Specimens of nerve terminals optimal for conventional electron microscopy are obtained when the tissue is sectioned in the range of 50–100 nm in thickness. Vesicles are sectioned in a random orientation; some vesicles are transected at various planes, while others reside within the section and between the sectioning planes, depending on the section thickness and vesicle dimensions. Determination of the spherical diameters offers stereological problems that need to be addressed in order to characterize the dimensions of the vesicles and the population of diameter measurements for comparative purposes. The measurement problem of spherical vesicles occurs when vesicles are sectioned at the caps, producing various sized projected circular images. When the center of the spherical vesicle resides within the section, the true diameter of the sphere will be observed in the projected image. The projection of the varying sized caps (when the center of the spherical vesicle lies outside the section) and the complete vesicles from 3-D space on to the 2-D viewing plane will result in observed circles of various diameters. Theoretically, the smallest of the vesicle caps should also be observable, but in practice this is not the case. So the observable data is degraded in at least two ways and does not represent the true distribution of the randomly sectioned vesicles.

Most investigators report the mean diameter of measured vesicles from electron micrographs, but if the distribution is made up of multiple sized vesicles with varying amounts in the sample, a ‘mean’ value represents a mixed population and includes the diameters of the ‘caps’ (degraded data). In order to better represent a mean for such distributions we make use of a mathematical approach that corrects for the biases in the diameters of the distribution. This study illustrates that obtaining a mean value from the measurable diameters within a combined distribution does not yield the true diameter of the actual vesicles in the sample, since fragments of the vesicles distort the distribution and because populations of vesicles with different mean sizes may be present. By correcting the distortion of the observed distribution of measurable vesicle diameters, a closer approximation of the true distribution is achieved.

## 2. Methods

We used electron micrographs of synapses obtained from the abdominal slow flexor muscle in the crayfish,

*Procambarus clarkii*, supplied by Atchafalaya Biological Supply Co. (Raceland, LA). Preparations were dissected in a modified Van Harreveld’s crayfish solution (Wojtowicz and Atwood, 1984). Procedures for processing for electron microscopy are described by Jahromi and Atwood (1974). Sections were collected on Formvar-coated slotted grids. A log of each serial section was kept and the thickness was determined by interference colors of the sections while they were floating on the surface of water after sectioning. Most sections were consistently cut at 75 nm. The sections were viewed and photographed on an electron microscope at a magnification of  $20\,600\times$  followed by printing at a magnification of  $7\times$ . Fig. 1 is an electron micrograph of a motor nerve terminal which illustrates the clear core vesicles that contain neurotransmitters and from which higher magnifications were obtained. Calibrations were made by the use of calibrated elec-

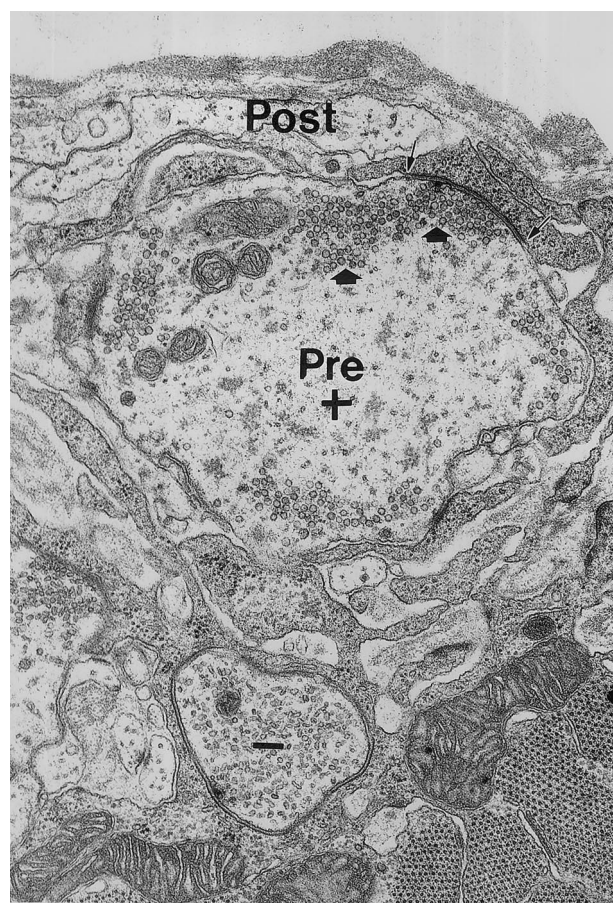


Fig. 1. An electron micrograph of a motor nerve terminal illustrating the clear core vesicles (arrow heads) which contain neurotransmitter. The presynaptic terminal of the excitor axon (Pre +) and an inhibitor axon (-) are shown. Only vesicles in the excitor are used in this study since they are spherical in shape as compared to oval vesicles contained in the inhibitor. The darkened pre- and post-synaptic membrane defines the synaptic site (arrows define the borders) in which these vesicles fuse during synaptic transmission. Scale bar is 250 nm.

tron microscopic grids for each magnification setting. Measurements of synaptic vesicle diameters were made by a single individual with the use of an eye micrometer. The outermost thickness of the vesicle membrane was taken as its diameter. To determine if the vesicles were of a uniform diameter, perpendicular measures were made across the projected vesicle image. The projected circles taken for this study were generally equidimensional. There were 933 data points collected in this study.

### 3. Results

The mathematical background for the stereological problems considered here are based on the assumption that spheres (neglecting the possibility of overlapping) are homogeneously distributed in three-dimensional space, and that observations are taken within a given random ‘slice’ through this space, defined by means of two parallel planes of distance  $2\mu$  apart. We let  $f(\cdot)$  denote the true density function for the radii of the spheres in three-dimensional space, and  $g(\cdot)$  denote the density function of the radii of the (orthogonally projected) circles observed within the slice. In order to deduce the relationship between  $f$  and  $g$ , it is useful to introduce the auxiliary density function  $p(\cdot)$  for the radii of those spheres that intersect with our ‘slice’. It is then easily argued that  $p(x)$  must be proportional to  $(2\mu + 2x)f(x)$ , corresponding to the fact that larger spheres are disproportionately more likely to be intersected by the slice. We can refer to this as ‘length-plus-thickness-biased sampling’, in analogy with the term ‘length-biased sampling’ as used, for example, in Vardi (1982). Next, if  $X = x$  is a given observation from  $p(\cdot)$ , and  $Y$  is the ‘corresponding observation’ from  $g(\cdot)$ , then simple geometrical reasoning shows that  $Y = x$  with probability  $2\mu/(2\mu + 2x)$  — corresponding to the case that the center of the sphere falls inside the slice — and  $Y = xZ$  with probability  $2x/(2\mu + 2x)$ , where  $Z = +\sqrt{1 - U^2}$  and  $U$  has the uniform distribution on  $[0, 1]$  and is independent of  $X$  — this latter corresponding to the case that the center of the intersected sphere falls outside of the slice. Based on these two facts alone, standard probability calculations can now be used to obtain the following well-known relationship which gives  $g$  as a function of  $f$ :

$$(\mu + m)g(y) = \mu f(y) + y \int_y^\infty \frac{f(x)}{\sqrt{x^2 - y^2}} dx \quad (1)$$

where

$$m = \int_0^\infty xf(x) dx$$

is the mean radius of the spheres in three-dimensional space. Further discussion of this stereological problem

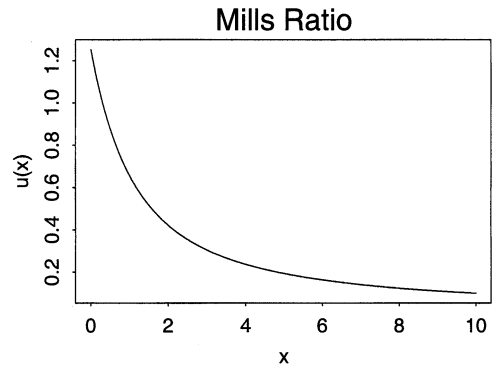


Fig. 2. Plot of Mills Ratio function  $u(x)$  on the interval  $[0, 10]$ .

may be found, for example, in Baddeley et al. (1986), Coleman (1979), Cruz-Orive and Weibel (1990), Feuerverger and Hall (2000), Hall and Smith (1988), Mecke and Stoyan (1980), Stoyan et al. (1987), Underwood (1970), and Weibel (1980).

Eq. (1) may be inverted. For example, Jakeman (1984) obtained the inversion formula

$$f(x) = -\sqrt{\frac{2}{\pi}} \frac{\mu + m}{\mu} \frac{d}{dx} \int_x^\infty u\left(\frac{\sqrt{2\pi(y^2 - x^2)}}{2\mu}\right) g(y) dy \quad (2)$$

where

$$u(x) = e^{x^2/2} \int_x^\infty e^{-t^2/2} dt$$

is the so-called Mills ratio. (This function, which is a simple transformation of the well-known error function, is the ratio of the probability of exceeding  $x$  to the density function at  $x$  for a standard Gaussian random variable.) We note that on  $[0, \infty)$  the function  $u(\cdot)$  is convex, strictly decreasing, takes on the value  $u(0) = \sqrt{\pi}/2$  at the origin, and has tails described by the well-known asymptotic (as  $x \rightarrow \infty$ ) expansion

$$u(x) \sim \frac{1}{x} - \frac{1}{x^3} + \frac{1 \cdot 3}{x^5} - \frac{1 \cdot 3 \cdot 5}{x^7} + \dots \quad (3)$$

A plot of the function  $u(x)$  is shown in Fig. 2. Eq. (2) leads directly to two alternative forms, the first of which,

$$\begin{aligned} \frac{\mu}{\mu + m} f(x) = g(x) \\ + \sqrt{\frac{2}{\pi}} \int_x^\infty \frac{x}{y} g(y) dy u\left(\frac{\sqrt{2\pi(y^2 - x^2)}}{2\mu}\right) \end{aligned} \quad (4)$$

is based on densities (here  $d_y$  is the differential in the variable  $y$ ) and the second of which

$$F(x) = 1 - \sqrt{\frac{2}{\pi}} \frac{\mu + m}{\mu} \int_x^\infty u\left(\frac{\sqrt{2\pi(y^2 - x^2)}}{2\mu}\right) dG(y) \quad (5)$$

is based on the corresponding cumulative distribution functions. In deriving Eq. (4), we used the easily ver-

ified fact that the derivative  $u'$  of Mills ratio satisfies  $u'(x) = x u(x) - 1$ . Note that the term  $x/y$  appearing in the integrand of Eq. (4) is bounded above by unity there, and therefore will not cause any numerical difficulties. Alternative, but equivalent, inversion formulae have also been given by Bach (1967, 1976), Goldsmith (1967), and others.

In practice we usually do not wish to make assumptions about the functional form of the density  $f(\cdot)$ ; we wish to let the data ‘speak for itself’ and therefore to carry out the analysis ‘non-parametrically’. However in actual electron microscopy experimentation there occurs the inevitable phenomenon of data degradation in the vicinity of the smaller observations so that the smaller observations are either not recorded, or are only recorded incompletely. It is essential to appreciate that there cannot be any fully satisfactory method to altogether eliminate this difficulty from a non-parametric analysis since we have, in effect, no data at all concerning spheres whose radii fall within this small-radius zone. Hence, in particular, there cannot be a resolution of this problem possessing demonstrable statistical optimality properties such as consistency or efficiency in the non-parametric context. Interestingly, however, the equations that link the 2-D and 3-D densities together are seen to each have the following remarkable property: except for the presence of the unknown constant quantity  $m$  which appears in the multiplicative proportionality factors, the value of the density function at any particular point depends on the value of the other density function only at that point and at the points **above** that point (and not on any of the points **below** that point). This holds true regardless of which direction one goes in — whether from  $f$  to  $g$  or from  $g$  to  $f$ . As a consequence, it fortunately is possible to *consistently* estimate the *shape* of the 3-D density function  $f(x)$  above that point  $x_0$  (say) below which the degradation phenomenon starts to occur; the only error resulting there (so far as consistency of the procedure is concerned) will be in the normalization constant, since it involves the true 3-D mean  $m$  which *cannot* be consistently estimated due to the absence of small-radius measurements. We can however consistently estimate the mean radius (in both the 2-D and the 3-D contexts) *conditionally* upon their lying above the degradation boundary.

Eqs. (2)–(5), although precise mathematically, are not statistically stable and therefore cannot be applied directly by using data-analogues in place of the unknown quantities involved. Our focus in this article is on three different and new approaches to this numerical and statistical inversion problem. These methods were applied to our data set obtained from thin sections of the neuromuscular junctions of the abdominal flexor in the crayfish. Data were pooled from five different sections of the same tissue which consisted of 933 observa-

tions of visible vesicle profiles; section thickness was  $2\mu = 75$  nm. The minimum and maximum of these observations on radii were 11.6 and 33.35 nm, respectively, and the mean is 20.39 nm. A histogram for this (uncorrected) data set is given in Fig. 3.

The first of these new methods is the so-called *implicit inversion* approach whose definition was first given, and theoretical properties investigated, in Feuerverger and Hall (2000) where further details are given. To describe this method, suppose that we wish to estimate the unknown true density  $f$  by means of a *histogram* density estimator  $\bar{f}$ , having a bin-width  $h$  say. (Such an estimator is defined as just being a density function which is constant on each of the intervals  $(0, h)$ ,  $(h, 2h)$ ,  $(2h, 3h)$ , and so on.) Now one desideratum would be to select  $\bar{f}$  to be that histogram (of bin-width  $h$ ) which is closest to  $f$  in the sense of minimizing the least-squares criterion function

$$\gamma(\bar{f}, f) \equiv \int (\bar{f} - f)^2 = \int \bar{f}^2 - 2 \int \bar{f}f + \int f^2 \quad (6)$$

Following now a standard statistical argument, since the last term on the far right is independent of  $\bar{f}$ , it may be omitted from the minimization problem. On the other hand the first term there does not depend on the unknown  $f$  and so is readily computable. The integral at the middle, however, is in effect just the expectation  $E\bar{f}(X)$  where  $X$  is distributed according to the  $f$  density. However due to the nice linear nature of Eq. (4), the expectation  $E\bar{f}(X)$  can be converted (on substitution, and by means of a simple calculation involving a change in the order of integration) to an expectation of the form  $E\beta(Y)$  where the random variable  $Y$  is distributed according to density function  $g$ . In fact, the function  $\beta$  turns out to be given by

$$\beta(y) = \frac{\mu + m}{\mu} \left\{ \bar{f}(y) - \sqrt{\frac{2}{\pi}} \int_0^y \bar{f}(x) d_x u \left( \frac{\sqrt{2\pi(y^2 - x^2)}}{2\mu} \right) \right\}$$

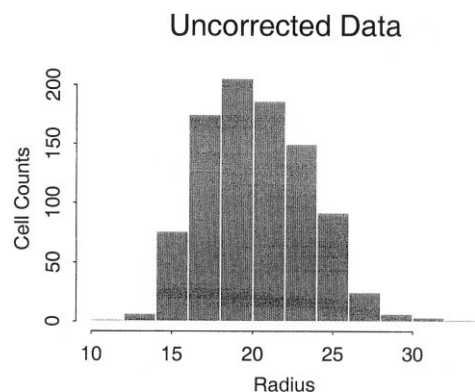


Fig. 3. A histogram of the raw (uncorrected) data set; sample size is  $n = 933$ ; section thickness is 75 nm. The data are radii of synapses from the abdominal slow flexor muscle in the crayfish *Procambarus clarkii*.

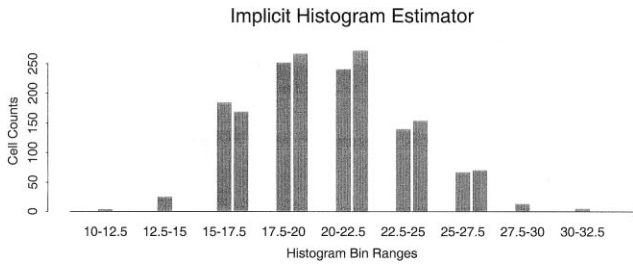


Fig. 4. A superposition of two histograms using the data of Fig. 2. The left-most bar of each bin corresponds to the raw (uncorrected) data, while the right-most bar corresponds to the (corrected) histogram as estimated by the ‘implicit’ inversion procedure described in the text.

so that an estimate of  $E\bar{f}(X)$  may then be obtained as

$$\frac{1}{n} \sum_{i=1}^n \beta(Y_i)$$

Substituting this estimate into Eq. (6) in the obvious way, the solution  $\bar{f}$  of the resulting ‘estimated’ quadratic minimization problem may now be determined using standard quadratic programming algorithms. A formula for estimating  $m$  may be obtained using an analogous calculation, by means of which the expectation integral  $m = \int xf(x) dx$  is converted into an expectation integral of the form  $\int v(y)g(y) dy$ . Solving for  $m$  in the resulting equation then leads to

$$m = \frac{\mu E[v(Y)]}{\sqrt{\frac{\pi}{2}} \mu - E[v(Y)]} \quad (7)$$

where

$$\begin{aligned} v(y) &= \int_0^y u \left( \frac{\sqrt{2\pi(y^2 - x^2)}}{2\mu} \right) dx \\ &= y \int_0^1 u \left( \frac{y\sqrt{2\pi(1 - z^2)}}{2\mu} \right) dz \end{aligned}$$

and the estimator,  $\hat{m}$ , is obtained from Eq. (7) by replacing  $E[v(Y)]$  there by the sample average

$$n^{-1} \sum_{i=1}^n v(Y_i)$$

The theory and further details of this procedure are given in Feuerverger and Hall (2000).

The implicit inversion method described above was applied to our data set using a histogram bin width of  $h = 2.5$  nm. The mean radius, as determined by the method of Eq. (7) was 22.28 nm (as compared with 20.39 nm for the raw data). The resulting histogram estimator is shown in Fig. 4. In fact, in this figure, two histograms are shown superimposed; within each of the bin ranges shown, the left-most bar corresponds to the histogram value for the raw data, while the right-most bar corresponds to the histogram value for the implicit inversion estimator. Essentially no mass (i.e. density mass) occurred outside of the bin ranges shown. It may

be seen that the correction procedure has the effect of shifting mass upwards. Thus in the lowest bins [(10, 12.5) and (12.5, 15)] no mass is assigned to the corrected histogram, while in the (15 – 17.5) bin, the mass in the corrected histogram is less than for the raw data. On the other hand, the next four bins all show increased mass assigned by the corrected estimator. For this data set, the corrected histogram turns out not to assign any noticeable mass to the top two bins — a consequence of the very low mass located within those bins, together with the vagaries of the mean squared error criterion on which the procedure is based.

The method described and implemented above is *implicit* in the sense that the optimality measure of the estimate  $\bar{f}$  has been ‘referred back’ by means of the criterion function (Eq. (6)) to the ‘inverse space’ of the spheres rather than to the ‘direct space’ of the circles. An *explicit* approach, described for example in Feuerverger and Hall (2000), may be based on Eq. (4) by simply replacing  $g$  there by a ‘kernel density estimator’

$$\hat{g}(y) = \frac{1}{nh} \sum_{i=1}^n K\left(\frac{y - Y_i}{h}\right)$$

where  $K$  is an appropriate ‘kernel function’ and  $h$  is a ‘bandwidth’, and by carrying out the integration numerically. We applied this procedure to our data using the standard Gaussian kernel function  $K(x) = (2\pi)^{-1/2} \exp(-x^2/2)$  and bandwidth parameter  $h = 1$  nm. Fig. 5 shows a superposition of the resulting kernel density estimator  $\hat{g}$  for the raw data (dotted line) and the density estimator obtained in this way via Eq. (4) for  $f$  (solid line). Since the estimator  $\hat{g}$  does not technically lie in the function space of possible 2-D distributions for this problem, the estimated  $f$  is seen to take on some negative values (at the lower range). This effect is exacerbated by the low-radius ‘data-degradation’ phenomenon discussed earlier. Nevertheless, it is seen that the correction procedure is shifting density mass upwards, and as we have discussed, the ‘shape’ of  $f$  is being estimated correctly above the point below which data-degradation begins to occur.

Our third approach involves substituting the cumulative distribution function  $G(y)$  in Eq. (5) by its empirical version  $G_n(y)$ , where  $G_n(y)$  equals the proportion of the observations less than or equal to  $y$ . It turns out that it is not difficult to prove that this procedure is in fact consistent, so that — for large sample sizes at least — the resulting estimator for  $F$  will (at each point  $x$ ) become close to its true value. The difficulty with this procedure in practice, however, is that the resulting estimator of  $F$  will typically not be a non-decreasing function, and, further, will typically fall outside of its mandatory  $[0, 1]$  range. Some examination of the issues here is instructive. The empirical distribution function  $G_n(y)$  is just an average of Heavyside functions — one

## Explicit Density Estimator

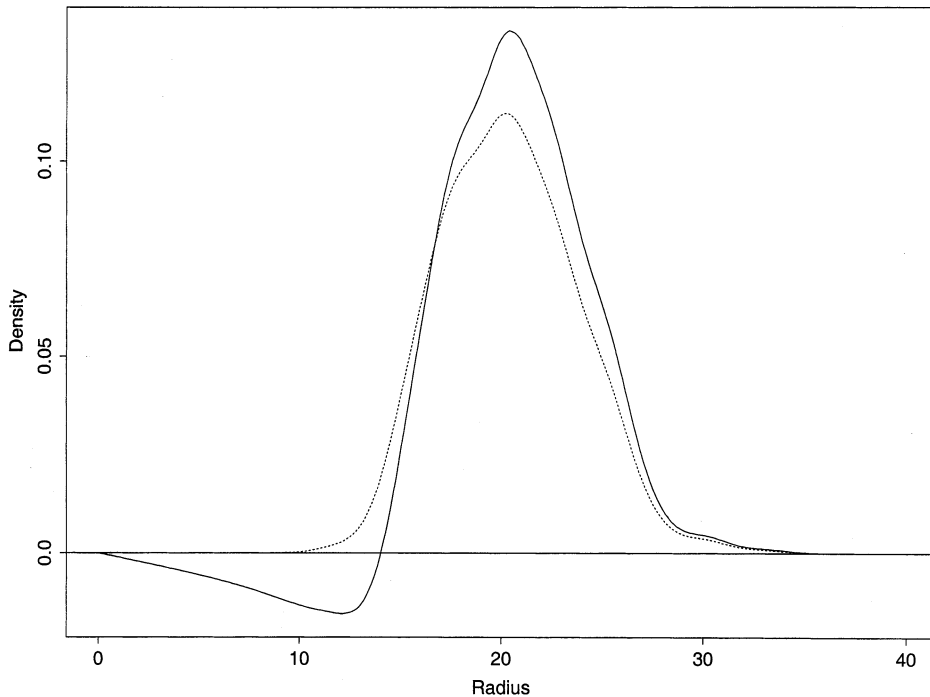


Fig. 5. Density estimators for the data of Fig. 2. The dashed curve is the kernel density estimator for the raw data based on a standard Gaussian kernel with bandwidth  $h = 1$ ; the solid curve is the explicitly inverted (corrected) density estimate described in the text.

for each datum. A typical such Heaviside function,  $H(y)$  say, will take on the value 0 when  $y$  lies below the datum, and the value 1 otherwise. Thus when  $G_n(y)$  is substituted for  $G(y)$  in Eq. (5), since  $G_n(y)$  enters linearly in this formula, the result will just be the superposition (or average) of terms resulting from the individual Heaviside functions. Fig. 6 shows a typical  $F(x)$  computed using Eq. (5) using just a single datum in place of  $G(y)$ , i.e. using a Heaviside function corresponding to one particular observation. It is seen that the resulting function is not monotone increasing — and has monotone tendency only in the roughest sense — and even falls below 0. The location of the ‘drop’ in this resulting function is determined by the value of the datum.

In the case of our data, when all of these resulting component curves are averaged, we obtain the ‘empirical estimator’ shown in Fig. 7. This cumulative distribution function estimator falls below 0 — again partially due to the data degradation phenomenon, and it is not strictly increasing, even (as may be seen on close inspection of the graph) in the upper ranges for radii. A natural resolution for these problems would be to ‘isotonize’ the estimator — that is, to replace the estimated  $F$  by that function which satisfies the required monotonicity and  $[0, 1]$  range constraints, and which is closest to it in the distance defined by the integrated squared difference between functions. Such an isotonicizing ‘fitting’ procedure may be carried out, for example,

by means of an iterated convex minorant algorithm as described, for example, in Robertson et al. (1988).

In fact, this is the approach that was proposed by Groeneboom and Jongbloed (1995) and by Jongbloed (1995, 2000) in their investigations into the ‘thin-slice’ version of the Wicksell inversion problem. (In contrast to the thin-slice problem, note that our data derives from a ‘thick-slice’ experiment in the sense that it involves a slice whose thickness is comparable to the observations themselves, and therefore cannot be regarded as a slice of zero thickness.) In their context,

## One Component

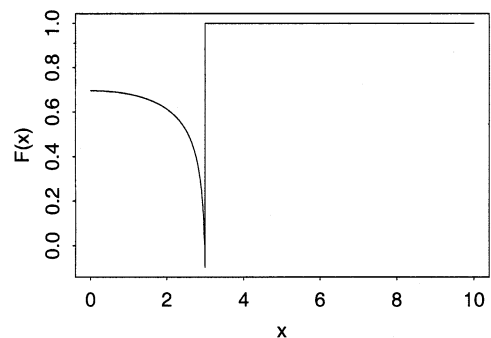


Fig. 6. A typical cumulative distribution function estimator  $F$  obtained from Eq. (5) when  $G$  there is replaced by a Heaviside function, i.e. by an empirical cumulative distribution function based on a single data point.

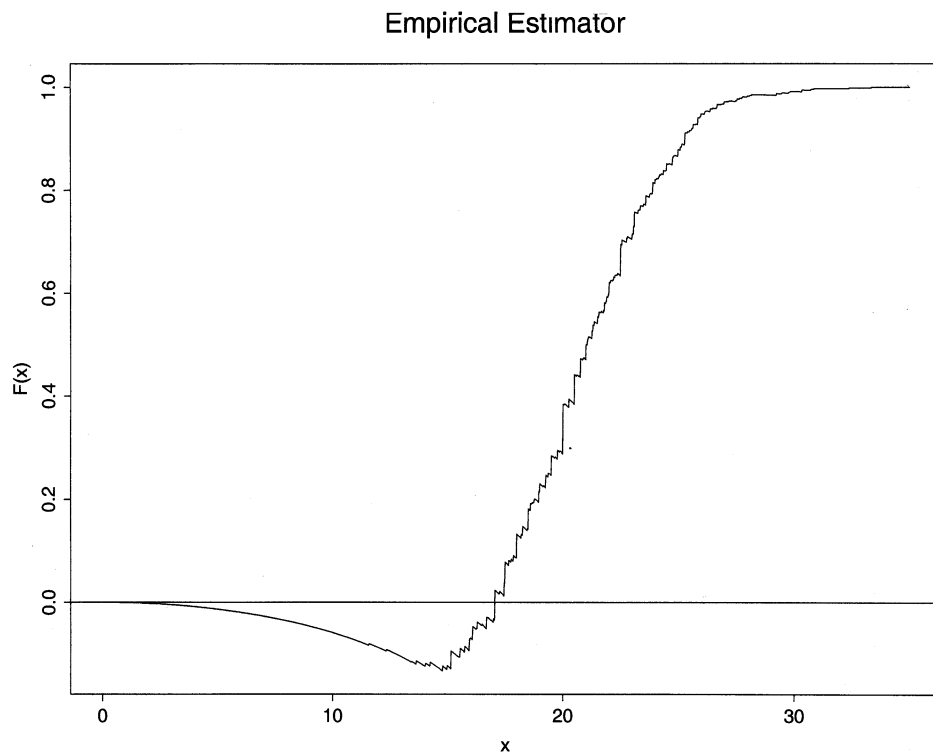


Fig. 7. Empirical estimator of  $F$  obtained from Eq. (5) when  $G$  there is replaced by the empirical distribution function of the raw data used in Fig. 2.

Groeneboom and Jongbloed prove not only the point-wise consistency of the raw estimator, but also the uniform consistency of their isotonizing procedure. They also prove, by detailed calculations, the very remarkable result that the mean squared error of their isotonized estimator is exactly one half that of the raw estimator. In our present ‘thick-slice’ context, the raw estimator (as in Fig. 7) is itself already uniformly consistent (unlike the thin-slice case) and it is clear that the isotonized version will also result in gains in efficiency. We implemented the isotonizing step using a convex minorant algorithm for our data and obtained the estimator shown in Fig. 8. Finally, Fig. 9 gives the histogram estimator obtained directly from the isotonized distribution function estimator of Fig. 8. In Fig. 9 we have again superimposed the raw histogram estimator as the left-most bar in each of the bins. It is seen that this estimator deletes the density mass in the first two bins and substantially reduces the mass in the third bin. In all higher bins, mass is added.

The computations described in this section were carried out using the S-Plus statistical computing package; see for example, Becker et al. (1988). The quadratic programming module used was ‘quadprog’ and the iterated convex minorant module used was ‘monsmo’ — both available from the Carnegie Mellon University ‘statlib’ website.

#### 4. Discussion

The amount of transmitter contained within a vesicle is one of the key factors which determines the degree of transmission from one cell to another. The amount of neurotransmitter in a vesicle is believed to be related to the size of the vesicle (Zhang et al., 1998). Due to the small sizes of synaptic vesicles (40–60 nm diameters) at the crayfish NMJ, electron microscopic techniques provide the only approach to image the vesicle dimensions. Obtaining the true dimensions of synaptic structures is complicated by stereological considerations of obtaining sections of an object in 3-D space and observing the projected image on a 2-D plane (Atwood and Cooper, 1996).

The distribution in the occurrences of the projected diameters used in this study revealed two obvious features: (1) the population is not made up of vesicles of uniform diameter, since there is a right-hand shoulder of the distribution; and (2) there is degradation in the data set on the left-hand side of the distribution because of the limits of resolution. In this study, we chose to focus on determining a method to better determine a mean size and distribution of the population of vesicle diameters associated with measurements obtained from photomicrographs of electron microscopic images. In doing so, three mathematical processes were utilized, an implicit inversion of the data set; an explicit approach; and substitution of a cumulative distribution function

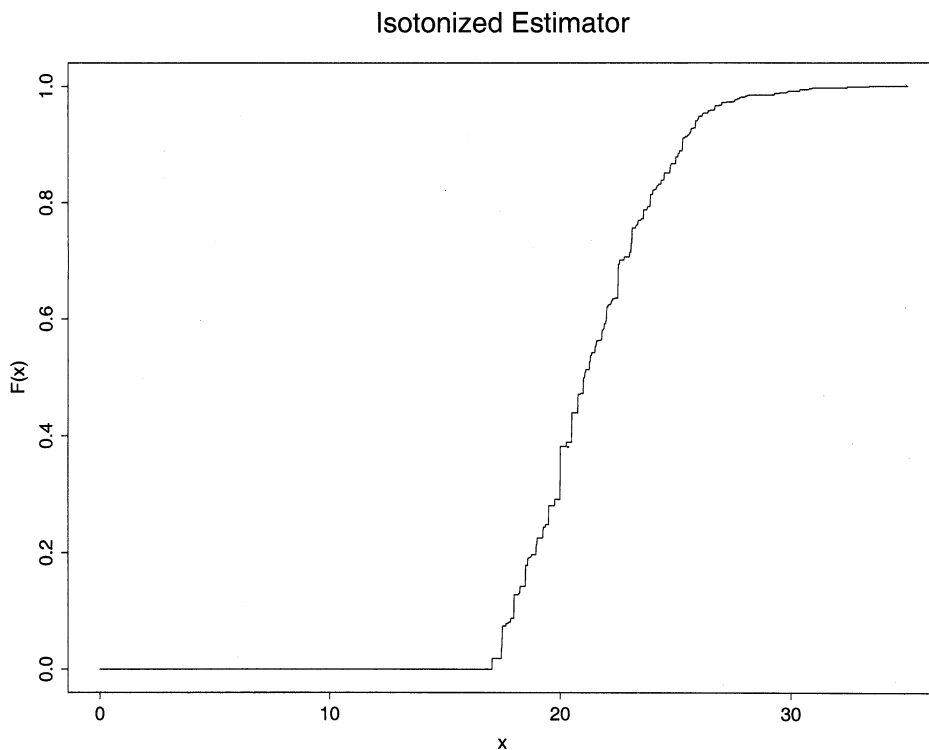


Fig. 8. Isotonized version of the estimator shown in Fig. 6 obtained by applying a convex minorant algorithm.

for the empirical distribution together with isotonization. These procedures provided distributions of the measurable data set that more correctly represent the true data set within the population, and thus provide an ability to calculate an improved estimate of the mean of the true distribution for comparisons to other data sets of vesicle diameter measures.

Estimating the 3-D dimensions of non-spherical structures from series of 2-D images has received attention over the years (DeGroot and Bierman, 1982; Gundersen and Jensen, 1983; Atwood and Cooper, 1996). Even to estimate the dimensions of ellipsoids of near-spherical shape is not a trivial matter (Cruz-Orive, 1980). The determination of spherical diameters is a simpler problem but still complex if the spherical populations are not homogeneous in diameter (Cruz-Orive, 1980; Clark and Moore, 1983).

Some of the variables that have an effect in determining the 3-D dimensions of vesicles from 2-D distributions of observed vesicle diameters are: (1) the thickness of the sections; (2) the degree of electron density of the vesicle membrane; (3) the uniformity in the dimensions of the vesicles; and (4) the dimensions of the vesicle in relation to the section thickness. Stereological corrections of the nature proposed here will clearly be particularly important when comparing data sets derived under different section thicknesses and/or under different underlying population distributions.

Various fixation procedures of aldehydes and solutions of differing osmolarity have been shown to alter

the observed synaptic vesicle profile distributions (Fox, 1988). In standard fixation procedures of crustacean motor nerve terminals, the vesicles of excitatory nerve terminals are more equidimensional than vesicles from inhibitory terminals (Uchizono, 1967; Atwood and Morin, 1970; Komuro, 1981), but with freeze-substitution fixation procedures, the difference in shape is not observed (Nakajima and Reese, 1983; Atwood and Tse, 1993). Thus, freeze-substitution fixation may give the most reliable preservation of the vesicles' true dimensions if future studies are to be made in this area. Additionally, Fox (1988) showed that the largest error in determining vesicle profile distributions resulted from reader bias by various people sampling the same set of data. In our case, the same individual measured all the data sets. By taking various-sized data sets, Fox (1988) found that 200 vesicles profiles were sufficient to obtain

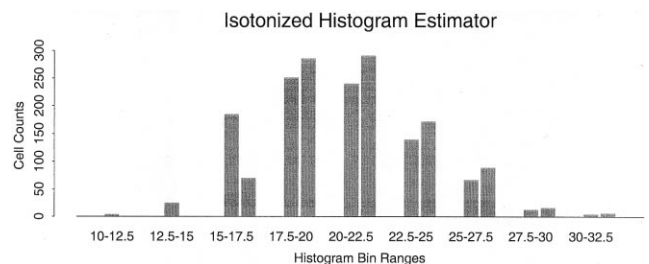


Fig. 9. A superposition of two histograms: left-most bar in each bin represents raw data as in Fig. 2, right-most bar is histogram obtained from the isotonized estimator shown in Fig. 7.

Table 1  
Means and medians of the data (radii) before and after analysis

Estimator	Mean	% Difference	Median
Raw mean	20.39		20.03
Implicit	22.28	9.27	20.27
Isotonized	21.27	4.32	20.95

an adequate estimate of the mean size and profile distribution. This would be preparation-dependent because of the possible variability in true size of the vesicles. Another possible factor that may result in variation among sections of the same tissue is the stretching of the thin sections induced by the electron beam of the microscope. This problem is related to the thickness of the section. Periodic calibration of the electron microscope for alignment can relieve instrumental error but there may be variation among instruments. While stereological corrections are in all cases advisable, note that in the present study we do not deal with issues arising out of reader bias or out of use of multiple tissue samples which, of course, require additional statistical tools (e.g. Fox, 1988).

One comparison of the various approaches used here is reported in Table 1 which gives mean radii determined three ways: (1) using the raw data, (2) as determined by our 'implicit' approach, and (3) as determined by our isotonizing procedure. The mean values for the observed distribution is seen to be smaller than that of the isotonized distribution by 4.32% and of the implicit estimation procedure by 9.27%. Theory for determining S.E. for the means estimated via the implicit and isotonizing procedures has not yet been developed, but these could be estimated via the computer-intensive 'jack-knife' method. However a rough indication of the S.E. of these estimators is given by the S.E. of the raw mean radius as determined by the usual formula  $S/\sqrt{n}$ , where  $S$  is the sample S.D., and  $n$  is the sample size — this value is 0.109, or 0.53% of the raw mean value. Note, however, that this measure of accuracy makes no allowance for the effects of data degradation at small radii. Table 1 also gives the median for the raw distribution, and for the distributions obtained via the implicit and isotonizing procedures. Here the isotonized median is farther away from the raw median than is the implicit median, reflecting the significant non-symmetries of the underlying distributions.

The present study also stresses that one should not present just the mean of the observed vesicle diameters to describe a population of vesicles within a nerve terminal, but that it is better to present the distribution of the measurable projected diameters. This provides a better representation of the degraded distribution, thus providing a better index to compare among distributions. In addition, if comparative studies are to be

made among nerve terminals to assess intrinsic differences or differences due to experimental manipulations, the complete distribution of projected vesicle images should be presented. This improved measure affects the estimate volume, since the volume is  $4/3\pi r^3$ , where  $r$  is the radius. In turn it is the volume which limits the amount of transmitter that can be packaged within the vesicle, thus regulating the degree of the postsynaptic response.

## Acknowledgements

We thank Leo Marin for tissue processing and photomicrographs of tissue, and Brenda Crowe for programming assistance. Funded by NSERC-Canada (A. Feuerverger), NSF grant IBN-9808631 (R.L. Cooper) and MRC-Canada (H.L. Atwood).

## References

- Atwood HL, Cooper RL. Functional and structural parallels in crustaceans and *Drosophila* neuromuscular systems. *Am Zool* 1995;35:556–65.
- Atwood HL, Cooper RL. Assessing ultrastructure of crustacean and insect neuromuscular junctions. *J Neurosci Methods* 1996;69:51–8.
- Atwood HL, Morin WA. Neuromuscular and axoaxonal synapses of the crayfish opener muscle. *J Ultrastruct Res* 1970;32:351–69.
- Atwood HL, Tse FW. Physiological aspects of presynaptic inhibition. *Adv Neur Sci* 1993;1:19–65.
- Bach G. Kugelgrößenverteilung und Verteilung der Schnittkreise, ihre wechselseitigen Beziehungen und Verfahren zur Bestimmung der einen aus der anderen. In: Weibel ER, Elias H, editors. *Proceedings of the Symposium on Quantitative Methods in Morphology*. Berlin: Springer, 1967:23–45.
- Bach G. Über die Auswertung von Schnittflächenverteilungen. *Biom J* 1976;18:407–12.
- Baddeley AJ, Gundersen HJG, Cruz-Orive LM. Estimation of surface area from vertical sections. *J Microsc* 1986;142:259–76.
- Becker RA, Chambers JM, Wilks AR. *The New S Language*. Pacific Grove, CA: Wadsworth and Brooks/Cole, 1988.
- Clark KR, Moore MN. Unbiased linear property estimation for spheres, from sections exhibiting over projection and truncation. *J Microsc* 1983;131:311–22.
- Coleman R. *An Introduction to Mathematical Stereology*. University of Aarhus, Denmark: Department of Theoretical Statistics, 1979.
- Cooper RL, Feuerverger A, Menzinger M, Marin L, Atwood HL. Measurement problems associated with the reconstruction of synaptic structures at the electron microscopic level. *Abstr Soc Neurosci* 1995a;21:709.5.
- Cooper RL, Marin L, Atwood HL. Synaptic differentiation of a single motor neuron: conjoint definition of transmitter release, presynaptic calcium signals, and ultrastructure. *J Neurosci* 1995b;15:4209–22.
- Cooper RL, Winslow J, Govind CK, Atwood HL. Synaptic structural complexity as a factor enhancing probability of calcium-mediated transmitter release. *J Neurophysiol* 1996;75:2451–66.
- Cruz-Orive LM. On the estimation of particle number. *J Microsc* 1980;120:15–27.

- Cruz-Orive LM, Weibel ER. Recent stereological methods for cell biology: a brief survey. *Am J Physiol* 1990;258:L148–56.
- DeGroot DMG, Bierman EPB. The complex-shaped ‘perforated’ synapse, a problem in quantitative stereology of the brain. *J Microsc* 1982;131:355–60.
- Fox GQ. A morphometric analysis of synaptic vesicle distributions. *Brain Res* 1988;475:103–17.
- Feuerverger A, Hall P. Methods for density estimation in thick-slice versions of Wicksell’s problem. *J Am Stat Assoc* 2000;95:535–46.
- Goldsmith PL. The calculation of true particle size distributions from the sizes observed in a thin slice. *Br J Appl Phys* 1967;18:813–30.
- Groeneboom P, Jongbloed G. Isotonic estimation and rates of convergence in Wicksell’s problem. *Ann Stat* 1995;23:1518–42.
- Gundersen JG, Jensen EB. Particle sizes and their distribution estimated from line- and point-sampled intercepts. Including graphical unfolding. *J Microsc* 1983;131:291–310.
- Hall P, Smith RL. The kernel method for unfolding sphere size distributions. *J Comput Phys* 1988;74:409–21.
- Jahromi SS, Atwood HL. Three-dimensional ultrastructure of the crayfish neuromuscular apparatus. *J Cell Biol* 1974;63:329–34.
- Jakeman AJ. Numerical inversion of a second kind singular Volterra equation — the thin section equation of stereology. *Utilitas Math* 1984;26:193–213.
- Jongbloed G. Three statistical inverse problems: estimators—algorithms—asymptotics. Ph.D. Thesis, Delft University of technology. Cip-data Koninklijke Bibliotheek, Den Haag, 1995.
- Jongbloed G. Sieved maximum likelihood estimation in Wicksell’s problem. Faculteit der Exacte Wetenschappen, Vrije Universiteit, Amsterdam, 2000, unpublished.
- Komuro T. Fine structural study of the abdominal muscle receptor organs of the crayfish (*Procambarus clarkii*). Sensory endings and synaptic structures. *J Neurocytol* 1981;10:27–43.
- Mecke J, Stoyan D. Stereological problems for spherical particles. *Math Nachr* 1980;96:311–7.
- Nakajima Y, Reese TS. Inhibitory and excitatory synapses in crayfish stretch receptor organs studied with direct rapid-freezing and freeze-substitution. *J Comp Neurol* 1983;213:66–73.
- Petukhov VV, Popov VI. Quantitative analysis of ultrastructural changes in synapses of the rat hippocampal field CA3 in vitro in different functional states. *Neuroscience* 1986;18:823–35.
- Probst JW, Ko CP. Correlations between active zone ultrastructure and synaptic function studied with freeze-fracture of physiologically identified neuromuscular junctions. *J Neurosci* 1987;7:3654–64.
- Robertson T, Wright FT, Dykstra RL. Order Restricted Statistical Inference. New York: Wiley, 1988.
- Stoyan D, Kendall WS, Mecke J. Stochastic Geometry and its Applications. Berlin: Akademie-Verlag, 1987.
- Uchizono K. Inhibitory synapses on the stretch receptor neurone of the crayfish. *Nature* 1967;214:833–4.
- Underwood EE. Quantitative Stereology. Reading, MA: Addison-Wesley, 1970.
- van de Goor J, Ramaswami M, Kelly R. Redistribution of synaptic vesicles and their proteins in temperature-sensitive shibire(ts1) mutant *Drosophila*. *Proc Natl Acad Sci USA* 1995;92:5739–43.
- Vardi Y. Nonparametric estimation in the presence of length bias. *Ann Stat* 1982;10(2):616–20.
- Weibel ER. Stereological Methods, vol. 2. Theoretical Foundations. London: Academic Press, 1980.
- Wojtowicz JM, Atwood HL. Presynaptic membrane potential and transmitter release at the crayfish neuromuscular junction. *J Neurophysiol* 1984;52:99–113.
- Wong K, Karunanithi S, Atwood HL. Quantal unit populations at the *Drosophila* larval neuromuscular junction. *J Neurophysiol* 1999;82:1497–511.
- Zhang B, Koh YH, Beckstead RB, Budnik V, Ganetzky B, Bellen HJ. Synaptic vesicle size and number are regulated by a clathrin adaptor protein required for endocytosis. *Neuron* 1998;21:1465–75.